Quantum and classical magnetic Bloch points

Vladyslav M. Kuchkin, * Andreas Haller, Štefan Liščák, Michael P. Adams, Venus Rai, Evelyn P. Sinaga, Andreas Michels, and Thomas L. Schmidt
Department of Physics and Materials Science, University of Luxembourg, L-1511 Luxembourg, Luxembourg

(Received 7 June 2024; accepted 3 February 2025; published 24 February 2025)

A Bloch point represents a three-dimensional hedgehog singularity of a magnetic vector field in which the magnetization vanishes. However, standard micromagnetic theory, developed for magnetic moments of fixed lengths, lacks full applicability in studying such singularities. To address this gap, we study a Bloch point in a quantum Heisenberg model for the case of spin-1/2 particles. Performing an exact diagonalization of the Hamiltonian as well as using density matrix renormalization group techniques, we obtain the ground state, which can be used to recover the corresponding magnetization profile. Our findings demonstrate a variation of the spin length in the quantum model, leading smoothly to zero magnetization at the Bloch point. Our results indicate the necessity of generalizing the classical micromagnetic model by adding the third degree of freedom of the spins: the ability to change their length. To this end, we introduce a phenomenological micromagnetic $\mathbb{S}^3$-model, which enables the description of magnets with and without Bloch point singularities.

DOI: 10.1103/PhysRevResearch.7.013195

I. INTRODUCTION

Bloch points (BPs) are micromagnetic singularities which were introduced by Feldtkeller [1] and Döring [2] in the 1960s. For a unit magnetization vector field $\boldsymbol{m} : \mathbb{R}^3 \to \mathbb{R}^3$, such a Bloch point represents a statically stable hedgehog solution, $\boldsymbol{m} = -\boldsymbol{r}/r$, with finite energy existing in the classical Heisenberg model. Since the magnetization of the BP does not approach a constant ferromagnetic background at $r \to \infty$, it represents, strictly speaking, a defect in the magnetic microstructure. To date, a plethora of spin textures hosting BPs have been theoretically predicted and experimentally found. The most prominent examples are hard magnetic bubbles with Bloch lines [3–5], chiral bobbers [6,7], lattices of bobbers [8], and as dipolar strings [9]. Recently, theoretical studies demonstrated a chain of BPs stabilized by screw dislocations [10], which might play a crucial role in the formation of hopfion rings [11,12] and other topological states [13,14]. These spin textures are intensively studied for information storage and as information carriers in future electronic devices [15–18].

At the same time, the dynamics of magnetization textures hosting BPs cannot be correctly described by a straightforward micromagnetic model because the singularity of the effective magnetic field at the center of the BP leads to a divergent Heisenberg exchange interaction $\boldsymbol{b}_{\text{eff}} \sim \nabla^2 \boldsymbol{m}$. As a consequence, BP dynamics is mainly studied in atomistic spin models, where strong interactions of the BP with the lattice have been reported [19,20]. There have been attempts to combine atomistic and micromagnetic approaches by considering multiscale grids [21], but this is a complex method that requires treating each BP separately. A more straightforward approach would be to generalize the micromagnetic description of such singularities by allowing magnetization vector fields of variable lengths [22]. In previous studies [23,24], such a variation of the magnetization was justified by the presence of thermal fluctuations, which play an important role close to the Curie temperature. However, the experimentally observed textures hosting BPs do not necessarily require high temperatures, so it seems that temperature should not play a crucial role. In our study, we stay within the framework of a micromagnetic theory, which treats all magnets below the Curie temperature as athermal [25,26]. Thus, the variation of the Euclidean norm of the spin expectation value, which we call spin length in the remainder of this paper, must be uniquely attributed to quantum fluctuations.

Our paper explores the BP singularity manifesting in the effective field near the center of the BP, which is essential for further study of the dynamics of such points. We show that the problem can be effectively resolved if one allows the magnetization to change its length. Hence, we propose an order parameter $\boldsymbol{n}$ with $|\boldsymbol{n}| \in [0, 1]$. Considering a more general quantum-mechanical Heisenberg model underlying the classical micromagnetic model allows us to demonstrate such a variation of the spin length explicitly. In this model, the wave function $|\psi\rangle$ of a particle with spin s can be used to calculate the magnetization vector $\boldsymbol{n} \in \mathbb{R}^3$ as the expectation value of the spin operator $\boldsymbol{S}$ according to $\boldsymbol{n} = \langle\psi|\boldsymbol{S}|\psi\rangle / \hbar s$ with $|\boldsymbol{n}| \in [0, 1]$.

To distinguish such a magnetization profile from the one obtained by Feldtkeller and Döring [1,2], we refer to these BPs as quantum and classical ones, respectively, and describe them by the order parameters $\boldsymbol{n}$ and $\boldsymbol{m}$. We illustrate this in

*Contact author: vladyslav.kuchkin@uni.lu

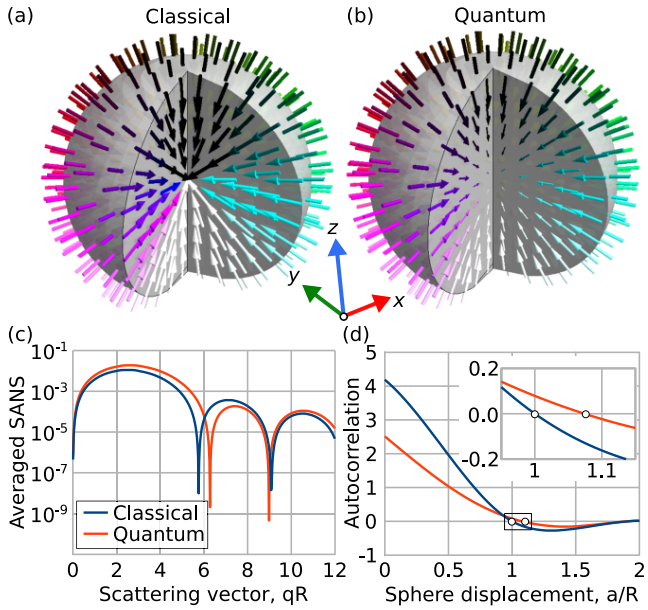

FIG. 1. Classical and quantum Bloch points. (a), (b) Magnetization vector fields for classical ($\boldsymbol{m} = -\boldsymbol{r}/r$) and quantum ($\boldsymbol{n} = -\boldsymbol{r}$) hedgehog solutions, respectively, in the vicinity of the BP core. The same color scheme for the spin visualization is used throughout the paper [27,28]. (c), (d) Analytical dependencies of the magnetic neutron scattering cross sections [see Eq. (7)] and their autocorrelation functions [see Eqs. (10) and (12)] obtained for these vector fields.

Figs. 1(a) and 1(b) for the hedgehog BP. For stabilization, both BPs must asymptotically exhibit a $-\boldsymbol{r}/r$ dependency for $r \to \infty$. As we show below, in the quantum case, this can be achieved by adding a Zeeman term near the boundary of the BP. It is worth highlighting that the common property shared by the classical and quantum BPs is their spherical symmetry. This can be written as $\boldsymbol{n}(\boldsymbol{r})/|\boldsymbol{n}(\boldsymbol{r})| = \boldsymbol{m}(\boldsymbol{r}) = -\boldsymbol{r}/r$ for $r > 0$. The main difference between the quantum mechanical and classical magnetization textures occurs near the BP core, where one has $\boldsymbol{n}(0) = 0$, while $\boldsymbol{m}(0)$ becomes undefined. We shall see below that for magnetic textures without singularities, order parameters $\boldsymbol{m}$ and $\boldsymbol{n}$ coincide.

Based on our results for the BP in a three-dimensional quantum Heisenberg model, we propose a generalized micromagnetic model which makes it possible to describe magnetic textures both with and without singularities. Since utilizing a regular Bravais lattice in the quantum-mechanical model would break the rotational symmetry of the BP, we will consider a special lattice geometry, based on concentric shells, for solving the quantum model. The generalized micromagnetic model we will introduce ensures a spherical symmetry with respect to the origin and can be applied to different magnetic systems characterized by isotropic exchange interactions. As we also show in Figs. 1(c) and 1(d), experimentally measurable quantities such as the magnetic neutron scattering cross section and its autocorrelation function, exhibit a clear difference between classical and quantum BPs.

The paper is organized as follows. In Sec. II, we introduce the quantum Heisenberg model and discuss possible geometries for placing spin-1/2 particles in 3D space that preserve the spherically symmetric profile of the BP. Section III presents the results of numerically solving the quantum model using exact diagonalization (ED) and the density matrix renormalization group (DMRG) method. Moreover, we introduce a classical generalized micromagnetic model that regularizes the BP singularities. The section ends with a comparison between classical and quantum BPs, quantities that are measurable in neutron scattering experiments. In Sec. IV, we discuss the importance of the introduced regularized model and some of its possible further applications. Finally, Sec. V summarizes the main findings of this paper.

II. BASIC MODEL

We start from the quantum Heisenberg model for a single shell of N interacting spin-1/2 sites placed equidistantly on a sphere. Each spin is represented by an operator $\boldsymbol{S}_i = \hbar\boldsymbol{\sigma}_i/2$ using a vector of Pauli matrices $\boldsymbol{\sigma}_i$, and the Hamiltonian reads

$$\mathcal{H}_1 = -J\sum_{\langle i,j\rangle} \boldsymbol{S}_i \cdot \boldsymbol{S}_j - J_c \sum_{i=1}^{N} \boldsymbol{S}_i \cdot \boldsymbol{h}_i. \tag{1}$$

The first term describes an intrashell ferromagnetic nearest-neighbor exchange coupling with a strength $J > 0$. To stabilize spherically symmetric BPs, we are limited to $N \in \{4, 6, 8, 12, 20\}$ for the number of sites per shell, corresponding to the Platonic solids [see Fig. 2(a)], with the respective number of bonds being $N_b \in \{6, 12, 12, 30, 30\}$. Using any other number of spins in a single shell will necessarily break the spherical symmetry and lead to a misorientation of the spins relative to the spherically symmetric hedgehog field. The environment of the shell is described by an effective Zeeman term with spherically symmetric magnetic field $\boldsymbol{h}_i = -\boldsymbol{r}_i/r_i$, where the $\boldsymbol{r}_i$ refer to the spin positions and $J_c > 0$ is an effective coupling constant.

In the case of multiple shells, the Hamiltonian (1) is generalized to

$$\mathcal{H}_{\mathrm{P}} = -J\sum_{\langle i,j\rangle,p} \boldsymbol{S}_i^p \cdot \boldsymbol{S}_j^p - J\sum_{i,\langle p,q\rangle} r_p^2 \boldsymbol{S}_i^p \cdot \boldsymbol{S}_i^q - J_c \sum_i \boldsymbol{S}_i^P \cdot \boldsymbol{h}_i, \tag{2}$$

where $p \in \{1, \ldots, P\}$ sums over all P shells, $r_p = p$ is the (dimensionless) radius of the pth shell, and the superscript of the spin operators $\boldsymbol{S}_i^p$ denotes the shell number. The last term in Eq. (2) involves only spins from the outermost ($p = P$) shell, which are coupled to the external magnetic field to satisfy the boundary condition mentioned above. The total number of spins is NP in this case. More details on the derivation of the multishell Hamiltonian (2) are provided in the Supplemental Material [29].

It is worth noting that in a Heisenberg model with different exchange coupling constants in a given shell, it would be possible to achieve a symmetrical BP even for $N > 20$. This would require a fine-tuning of the coupling constants in a given shell, taking into account the number of neighboring spins. However, the goal of this paper is to demonstrate the spin length reduction and its vanishing at the center for the quantum BP with a hedgehog-like magnetization distribution in space. As we show below, this property already holds for systems with N corresponding to Platonic solids and for different $P > 1$. Approaching the thermodynamic limit, $N \to \infty$ and $P \to \infty$, would require a more careful analysis and goes

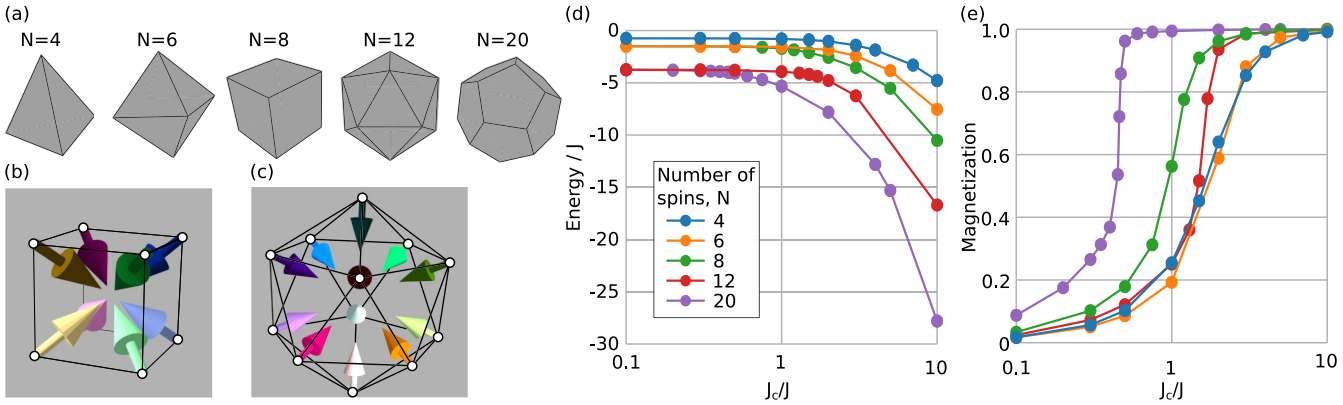

FIG. 2. Bloch point results for the single-shell case. (a) Platonic solids corresponding to equidistant points on the sphere. (b), (c) BP texture for the case of a cube ($N = 8$) and an icosahedron ($N = 12$), respectively. (d), (e) Energy (in units of J) and magnetization length $|\boldsymbol{n}|$ for different coupling parameters J_c/J.

beyond the scope of the current paper, but it is not necessary for observing how the quantum properties of the spins remove the singularity of the classical magnetization profile.

III. RESULTS

A. Single shell Hamiltonian

The ground state (GS) of the Hamiltonian (1) can be obtained by performing an ED for a sufficiently small number of lattice spins. The corresponding magnetic textures for the cube ($N = 8$) and the icosahedron ($N = 12$) cases are shown in Figs. 2(b) and 2(c). These examples are general, and we observe a similar ordering behavior of magnetic spins for all other cases depicted in Fig. 2(a). At the same time, the dependencies of the energy [Fig. 2(d)] and of the spin length [Fig. 2(e)] on the ratio J_c/J differ quantitatively due to the different number of spins and bonds in each case. In particular, for $J_c = 0$ the energy depends on the number N_b of interacting pairs according to $-JN_b/4$. In the strong-coupling limit ($J_c \gg J$), the energy is of the order of $-J_cN/2$.

Moreover, we have studied the simplest case of $N = 4$ (tetrahedron) analytically. We considered the limiting case of $J_c/J \to 0$ and calculated the energies of the GS and of the first four excited states in the Supplemental Material [29]. From this and from the obtained numerical results in Fig. 2, we can deduce the uniqueness of the GS for all $J_c/J > 0$. Since the systems for the other values of N shown in Fig. 2 are physically similar and obey the same symmetry, we do not expect any qualitative differences to the case $N = 4$.

B. Multiple-shell Hamiltonian

From the discussion of a single shell, we can infer that the physical properties are qualitatively similar for each N corresponding to a Platonic solid. This allows us to use the simplest case $N = 4$ to approach the thermodynamic limit $P \to \infty$ in the multishell Hamiltonian (2), which is required to describe the quantum BP in the bulk limit. To solve Eq. (2) numerically, we rely on ED and DMRG [30,31] methods. Both yield identical results for $P \in \{2, 3, 4, 5\}$ while DMRG remains computationally feasible even for $P > 5$.

In both cases, the corresponding magnetic texture reveals a spherically symmetric quantum BP with a spin length that decreases toward the origin, as highlighted in Fig. 3(b) for $J_c/J = 10$. This example is generic, and the profile $n(r) = |\boldsymbol{n}(\boldsymbol{r})|$ is always an increasing function of $r = |\boldsymbol{r}|$ with $0 \leqslant n(r) \leqslant 1$.

For a larger system with ten shells, we obtain the ground state using DMRG [see Fig. 3(c)]. We have examined different values of J_c/J and find that in the limit $J_c/J \gg 1$, the function $n(r)$ approaches a certain limiting curve, which we identify with the profile of the quantum BP. It is worth noting that the spins on the outermost shell show a reduced spin length ($|\boldsymbol{n}| < 1$) for any value of $J_c > 0$ and that they only approach the classical length ($|\boldsymbol{n}| = 1$) in the limit $J_c \to \infty$. This motivates us to use higher values of J_c for the DMRG simulations. Physically, the limit $J_c \to \infty$ corresponds to a quantum BP placed in a bath of classical spins where quantum fluctuations appear only for spins on the inner shells ($p < P$), while spins on the outermost shell ($p = P$) are classical. From the results of the numerical simulations, it follows that $|\boldsymbol{n}(r \to 0)| = 0$. Additionally, this fact correlates with general symmetry considerations—for an even number of spin-1/2 particles symmetrically distributed in space and subject to spherically symmetric boundary conditions, one can expect the magnetization to vanish at the origin. Guided by these results, we provide next a micromagnetic model that can be used to describe such BPs in systems of arbitrary geometry.

C. Micromagnetic $\mathbb{S}^3$-model

The constraint $0 \leqslant n(r) \leqslant 1$ can be written as an equality constraint by extending the order parameter to four dimensions by introducing a vector $\boldsymbol{\nu} \in \mathbb{S}^3$. Its first three components are given by the components of the vector $\boldsymbol{n}$, while the fourth one is determined by the length of $\boldsymbol{n}$,

$$\nu_1 = n_x, \quad \nu_2 = n_y, \quad \nu_3 = n_z, \quad \sqrt{1 - \nu_4^2} = |\boldsymbol{n}|. \tag{3}$$

As shown in Fig. 3(d), for a unique vector field $\boldsymbol{n}$, this definition allows for two possible fields $\boldsymbol{\nu}$, which differ by the sign of ν_4. To obtain a unique solution for the physical magnetization $\boldsymbol{n}$, we must require the generalized energy functional satisfies $\mathcal{E}[\boldsymbol{n}, \nu_4] = \mathcal{E}[\boldsymbol{n}, -\nu_4]$. Taking this into account, the

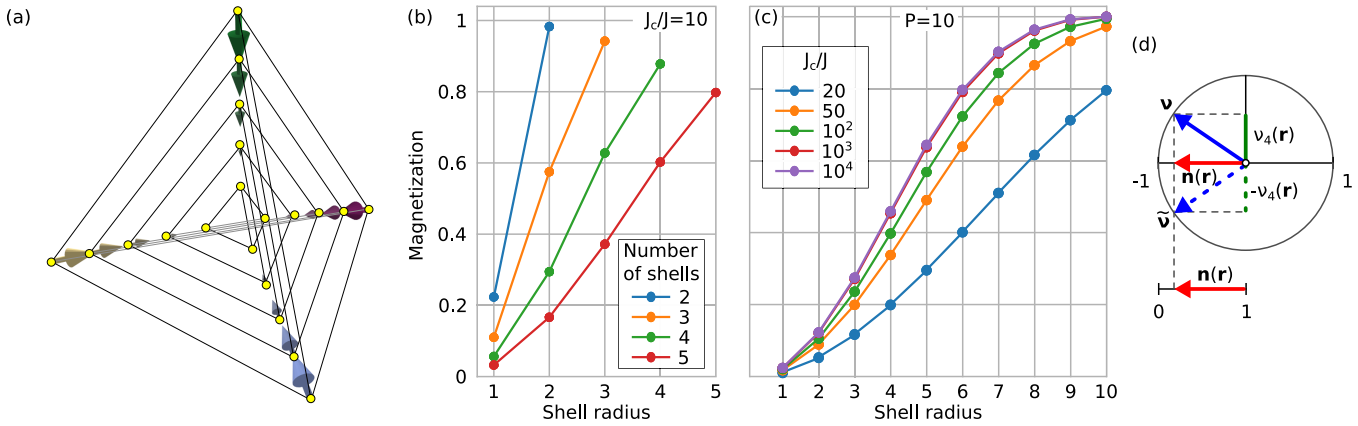

FIG. 3. BP results for the multishell case. (a) Quantum BP spin texture for the tetrahedral case with five shells. The bonds between interacting spins are shown. (b), (c) Dependency of the magnetization length on the shell radius. (b) corresponds to $P = 2, 3, 4, 5$ shells [Eq. (2)] with $J_c/J = 10$ (obtained using the ED method). (c) corresponds to $P = 10$ and $J_c/J = 20, 50, 10^2, 10^3, 10^4$ (obtained using the DMRG method). (d) illustrates the connection between the 3D vectors $\boldsymbol{n}$, with $|\boldsymbol{n}| \in [0, 1]$, and the 4D vector $\boldsymbol{\nu}$ with $|\boldsymbol{\nu}| = 1$. For a given $\boldsymbol{n}$, there are two vectors $\boldsymbol{\nu}$ and $\tilde{\boldsymbol{\nu}}$ with $\tilde{\nu}_4 = -\nu_4$.

classical $\mathbb{S}^3$ micromagnetic model we propose can be written in the following form:

$$\mathcal{E}[\boldsymbol{\nu}] = \mathcal{A} \sum_{i\in\{x,y,z\}} \int (\partial_i \boldsymbol{\nu})^2 dV + \kappa \int \nu_4^2 dV, \tag{4}$$

where $\mathcal{A}$ is the exchange-stiffness constant, and the last term with the coupling constant $\kappa > 0$ is introduced to make it possible to connect to the classical micromagnetic limit by using $\kappa \to \infty$, which leads to $\nu_4^2 = 0$ or equivalently $|\boldsymbol{n}| = 1$.

Following Ref. [2], we can now calculate the energy of the spherically symmetric quantum BP, which can be parametrized as

$$\boldsymbol{\nu} = \begin{pmatrix} \sin\theta\cos\phi\cos\psi \\ \sin\theta\sin\phi\cos\psi \\ \cos\theta\cos\psi \\ \sin\psi, \end{pmatrix}, \tag{5}$$

where $\theta(r)$ and $\phi(r)$ are spherical angles, and the function $\psi(r)$ defining the deviation from unit magnetization length satisfies the boundary conditions $\psi(r) = \pi/2$ for $r \to 0$ and $\psi(r) = 0$ for $r \to \infty$. Using this profile to perform the integral in the energy functional (4) over a ball of radius R, we obtain a result of the form $\mathcal{E}_{\mathrm{BP}} = 8\pi\mathcal{A}R + \Omega$. Here, Ω represents a negative contribution to the energy arising from the possibility of the spins changing their length [29]:

$$\Omega = 4\pi\mathcal{A}\int_0^R \left[(\psi')^2 + \left(\frac{\kappa}{\mathcal{A}} - \frac{2}{r^2}\right)\sin^2\psi\right] r^2 dr. \tag{6}$$

From the Euler-Lagrange (EL) equation, one finds the asymptotic limits of $\psi(r)$ as $\psi(r \ll 1) = \pi/2 - c_1^2 r/r^*$ and $\psi(r \gg 1) = (c_2^2 r/r^*)\exp(-r/r^*)$, where $r^* = \sqrt{\mathcal{A}/\kappa}$. In the Supplemental Material [29], we show that an ansatz of the form $\psi_a(r) = \arccos[\tanh(cr/r^*)]$ with a single fitting parameter c approximates very well the quantum BP profile arising from the EL equation.

As a consequence, the profile of a quantum BP is well described by a magnetization vector asymptotically reaching unit length exponentially, $|\boldsymbol{n}| \propto 1 - \exp(-r/\sqrt{\mathcal{A}/\kappa})/r$, for $r \gg 1$. This implies that the ratio $\sqrt{\mathcal{A}/\kappa}$ can be used to estimate the size of the quantum BP. Moreover, such an exponential localization means that the model (4) indeed coincides with the standard micromagnetic approach far from the BP singularity and modifies it only near the BP core.

D. Chiral bobber with a quantum BP

The simplest experimentally observed spin texture that hosts a BP is a chiral bobber. This state represents a skyrmion tube protruding into a ferromagnetic medium up to a certain depth and ending with a BP. In addition to the terms in Eq. (4), the Hamiltonian allowing the stabilization of such a state contains a Dzyaloshinskii-Moriya interaction (DMI) term of strength $\mathcal{D}$ [32,33] as well as an externally applied field. Choosing the strength of this field to be within the stability range of a chiral bobber, we can see as κ increases, the quantum BP shrinks and transforms into the classical BP solution (see Fig. 4). To obtain the stable chiral bobber, we minimized the energy with the conjugate gradient method as discussed in the Supplemental Material [29]. The vector field in the vicinity of the BP core coincides with that shown in Fig. 1(a) up to a rotation about the z axis by $\pi/2$.

Thus, the generalized model (4) can be supplemented by other terms, such as DMI and magnetic fields [26], relevant to the particular physical system. Moreover, even dipolar interactions can be straightforwardly included in the model because they do not require the conservation of the spin length. Previously proposed models that allow for a spin length variation included the Landau magnetic energy [34]. The main advantage of our $\mathbb{S}^3$-model as compared to the latter is that it naturally coincides with the standard micromagnetic approach for continuous magnetic vector fields and deviates only in the vicinity of BP singularities, so the magnetization always remains constrained by $|\boldsymbol{n}| \leqslant 1$.

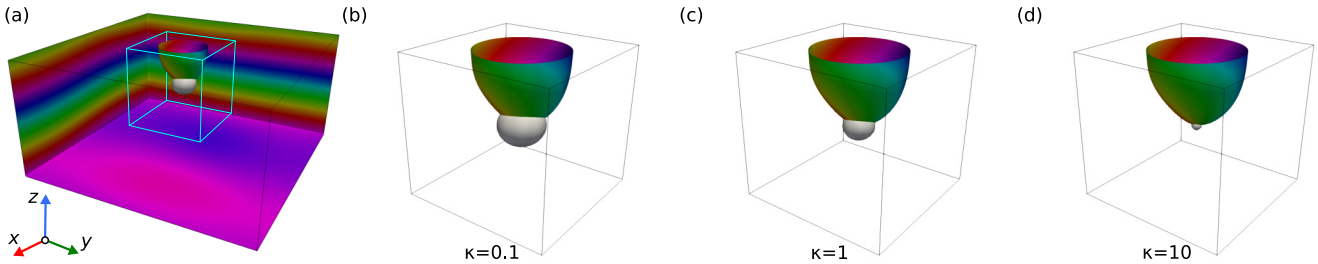

FIG. 4. Magnetization profile of a chiral bobber. (a) The relaxed chiral bobber stabilized at a magnetic field of $0.75\mathcal{D}^2/2M_s\mathcal{A}e_z$. Periodic and open boundary conditions were, respectively, assumed in the xy plane and along the z direction. The size of the light blue box is $4\pi\mathcal{A}/\mathcal{D} \sim 43$ lattice sites; the chiral bobber surface corresponds to spins with $n_z = 0$. The white ball corresponds to a magnetization length of $n = 0.95$, meaning that inside (outside) the ball one has $0 \leqslant n < 0.95$ ($0.95 < n \leqslant 1$). (b)–(d) The bobber for different values of the parameter κ given in units of $\mathcal{D}^2/2M_s\mathcal{A}$.

E. Experimental signatures of a quantum BP

For the BPs shown in Figs. 1(a) and 1(b), the magnetic neutron scattering cross sections can be obtained analytically (see Supplemental Material [29]). Here, we provide the results for the cross sections of the classical (I_1) and the quantum (I_2) BPs in a ball of radius R,

$$I_1 \simeq (qR\sin qR + 2\cos qR - 2)^2/(qR)^6,$$
$$I_2 \simeq (3qR\cos qR + ((qR)^2 - 3)\sin qR)^2/(qR)^8, \quad (7)$$

which are plotted in Fig. 1(c). To obtain a formula for I_1 and I_2, we rely on the BPs near-core magnetization vector fields $\boldsymbol{m} = -\boldsymbol{r}/r$ and $\boldsymbol{n} = -\boldsymbol{r}/R$, respectively. These expressions can be used straightforwardly to analyze experimental data and distinguish the classical BP from its quantum mechanical counterpart.

Considering the BP texture stabilized in a nanosphere, we can calculate the autocorrelation function of the magnetization $\boldsymbol{M}(\boldsymbol{r})$,

$$c(\boldsymbol{a}) = \int \boldsymbol{M}\left(\boldsymbol{r} - \frac{\boldsymbol{a}}{2}\right)\cdot\boldsymbol{M}\left(\boldsymbol{r} + \frac{\boldsymbol{a}}{2}\right)\mathrm{d}V, \quad (8)$$

where the total sphere displacement is given by vector $\boldsymbol{a}$ and the integration is over a volume given by the intersection of the two spheres. Without loss of generality, we use $\boldsymbol{a} = (0, 0, a)$. For a sphere of radius $R = 1$ and employing the quantum BP ansatz near the origin,

$$\boldsymbol{M}(\boldsymbol{r}) = \boldsymbol{n}(\boldsymbol{r}) = -\frac{(x, y, z)}{R}, \quad (9)$$

we obtain

$$c_1(\boldsymbol{a}) = \int\left(x^2 + y^2 + z^2 - \frac{a^2}{4}\right)\mathrm{d}V$$
$$= \frac{4\pi}{5}\left[1 - \frac{5}{2}\frac{a}{2} + \frac{5}{2}\left(\frac{a}{2}\right)^3 - \left(\frac{a}{2}\right)^5\right]. \quad (10)$$

An expression for $R \neq 1$ can be obtained from Eq. (10) via $c_1(\boldsymbol{a}) \mapsto c_1(\boldsymbol{a}/R)/R^2$. In contrast, for a classical BP with the profile

$$\boldsymbol{M}(\boldsymbol{r}) = \boldsymbol{m}(\boldsymbol{r}) = -\frac{(x, y, z)}{\sqrt{x^2 + y^2 + z^2}}, \quad (11)$$

we obtain

$$c_2(\boldsymbol{a}) = \int \frac{x^2 + y^2 + z^2 - a^2/4}{\sqrt{(x^2 + y^2 + z^2 + a^2/4)^2 - a^2z^2}}\mathrm{d}V$$
$$= \frac{4\pi}{3}\begin{cases} 1 - \dfrac{3a}{4} - a^2 + \dfrac{3a^3}{4}, & \text{for } 0 \leqslant a \leqslant 1 \\ -1 + \dfrac{1}{a} - \dfrac{3a}{4} + a^2 - \dfrac{a^3}{4}, & \text{for } 1 < a \leqslant 2. \end{cases} \quad (12)$$

The resulting functions $c_{1,2}$ are shown in Fig. 1(d). In the classical BP case, we have $c_2 = 0$ at $a = 1$ and $a = 2$. The former zero is due to the BP's spherical symmetry, and the latter corresponds to zero overlap of the spheres. In contrast, in the quantum BP case, one finds zeros of c_1 at $a \approx 1.07$ and $a = 2$. The change in the value of the first root is due to the possibility of spin length variation in a quantum case. Thus, this characteristic feature distinguishes classical and quantum BPs.

IV. PERSPECTIVE AND OUTLOOK

Many well-known magnetic materials, such as bcc Fe, hcp Co, fcc Ni, and hcp Gd, are characterized by isotropic exchange interactions. Moreover, the isotropic Heisenberg model can fairly well approximate the magnetic interactions of many compounds and alloys. Thus, the generalized Heisenberg model (4) represents an essential step toward the further study of BP properties in most magnetic materials. Possible extensions of this model can be considered by accounting for anisotropic exchange interactions relevant for multilayer systems [35] or by adding high-order frustration [36] and other SU(2) [37] terms. Although we focus on the simplest model featuring a BP singularity, follow-up studies that consider the role of such terms can be included in the micromagnetic $\mathbb{S}^3$-model in a straightforward manner. It is worth highlighting that in the standard micromagnetic model with frustrated exchange interactions, the classical BP has an infinite energy in any finite volume, irremovable by the choice of a spherical coordinate system. Therefore, the suggested effective $\mathbb{S}^3$-model also makes it possible to investigate BP properties in such magnetic systems.

Even though we do not investigate the dynamics in this paper, we want to outline briefly that the reported results naturally lead to an extended version of the Landau-Lifshitz-Gilbert (LLG) equation—the central equation of micromagnetism. The LLG equation relies on the effective field $\boldsymbol{b}_{\text{eff}}$, defined by the Hamiltonian, which is divergent at the BP core, as we mentioned before. For the case of spherically symmetric classical and quantum BPs, we can find effective fields analytically (see the Supplemental Material [29] for details). In particular, at $r \to 0$ one has $|\boldsymbol{b}_{\text{eff}}| \sim 1/r^2$ in the classical case and $|\boldsymbol{b}_{\text{eff}}| \sim r$ in the quantum case. As we can see, strictly speaking, the divergence of the effective field in the classical case makes the LLG equation inappropriate for describing the motion of classical BPs. In contrast, for the quantum BP the effective field remains continuous at the BP core, which makes it possible to derive generalized dynamics equations based on the same assumptions as in Landau and Lifshitz's original paper [25]. The minimization algorithm employed to find a stable chiral bobber represents pseudo-dynamics that shares many similarities with the dissipation dynamics provided by the LLG equation. We leave a detailed derivation of the precession dynamics and other dynamical torques LLG for future work [38].

Finally, we want to add that the suggested $\mathbb{S}^3$-model makes contact with Skyrme's original idea to describe baryonic matter [37]. Solitons in this model, called skyrmions, represent the distribution of the baryonic charge inside the nucleus. They are characterized by the homotopy group $\pi_3(\mathbb{S}^3)$. In this context, a quantum BP represents the simplest object which might be stable not only from an energetic but also from a topological point of view. Continuing the Skyrme model analogy, one can try to find magnetic materials that allow stable 3D topological states with the higher-order charges of the BP.

V. CONCLUSION

We have studied the BP singularity in the quantum Heisenberg model for spin-1/2 particles. The obtained magnetization vector field is characterized by a vanishing spin moment at the BP core. We suggested a generalized micromagnetic model for this quantum BP based on an $\mathbb{S}^3$ order parameter and applied this model to a chiral bobber. To experimentally distinguish a classical and a quantum BP, we have provided expressions for the magnetic neutron scattering cross sections and the corresponding autocorrelation functions.

ACKNOWLEDGMENTS

We acknowledge financial support from the National Research Fund Luxembourg under Grant No. C22/MS/17415246/DeQuSky. V.M.K. is grateful to N. S. Kiselev for fruitful discussions.

[1] E. Feldtkeller, Mikromagnetisch stetige und unstetige Magnetisierungskonfigurationen, Z. Angew. Phys **19**, 530 (1965).
[2] W. Döring, Point singularities in micromagnetism, J. Appl. Phys. **39**, 1006 (1968).
[3] A. P. Malozemoff and J. C. Slonczewski, *Magnetic Domain Walls in Bubble Materials* (Academic Press, New York, 1979).
[4] S. Da Col, S. Jamet, N. Rougemaille, A. Locatelli, T. O. Mentes, B. S. Burgos, R. Afid, M. Darques, L. Cagnon, J. C. Toussaint, and O. Fruchart, Observation of Bloch-point domain walls in cylindrical magnetic nanowires, Phys. Rev. B **89**, 180405(R) (2014).
[5] F. S. Yasin, J. Masell, Y. Takahashi, T. Akashi, N. Baba, K. Karube, D. Shindo, T. Arima, Y. Taguchi, Y. Tokura, T. Tanigaki, and X. Yu, Bloch point quadrupole constituting hybrid topological strings revealed with electron holographic vector field tomography, Adv. Mater. **36**, 2311737 (2024).
[6] F. N. Rybakov, A. B. Borisov, S. Blügel, and N. S. Kiselev, New type of stable particlelike states in chiral magnets, Phys. Rev. Lett. **115**, 117201 (2015).
[7] M. Redies, F. R. Lux, J.-P. Hanke, P. M. Buhl, G. P. Müller, N. S. Kiselev, S. Blügel, and Y. Mokrousov, Distinct magneto-transport and orbital fingerprints of chiral bobbers, Phys. Rev. B **99**, 140407(R) (2019).
[8] K. Ran, Y. Liu, Y. Guang, D. M. Burn, G. van der Laan, T. Hesjedal, H. Du, G. Yu, and S. Zhang, Creation of a chiral bobber lattice in helimagnet-multilayer heterostructures, Phys. Rev. Lett. **126**, 017204 (2021).
[9] G. P. Müller, F. N. Rybakov, H. Jonsson, S. Blügel, and N. S. Kiselev, Coupled quasimonopoles in chiral magnets, Phys. Rev. B **101**, 184405 (2020).
[10] M. Azhar, V. P. Kravchuk, and M. Garst, Screw dislocations in chiral magnets, Phys. Rev. Lett. **128**, 157204 (2022).
[11] F. Zheng, N. S. Kiselev, F. N. Rybakov, L. Yang, W. Shi, S. Blügel, and R. E. Dunin-Borkowski, Hopfion rings in a cubic chiral magnet, Nature (London) **623**, 718 (2023).
[12] Y. Liu and N. Nagaosa, Current-induced creation of topological vortex rings in a magnetic nanocylinder, Phys. Rev. Lett. **132**, 126701 (2024).
[13] V. M. Kuchkin and N. S. Kiselev, Homotopy transitions and 3D magnetic solitons, APL Mater. **10**, 071102 (2022).
[14] V. M. Kuchkin, N. S. Kiselev, F. N. Rybakov, I. S. Lobanov, S. Blügel, and V. M. Uzdin, Heliknoton in a film of cubic chiral magnet, Front. Phys. **10**, (2023).
[15] M. Beg, R. A. Pepper, D. Cortés-Ortuño, B. Atie, M.-A. Bisotti, G. Downing, T. Kluyver, O. Hovorka, and H. Fangohr, Stable and manipulable Bloch point, Sci. Rep. **9**, 7959 (2019).
[16] M.-Y. Im, H.-S. Han, M.-S. Jung, Y.-S. Yu, S. Lee, S. Yoon, W. Chao, P. Fischer, J.-I. Hong, and K.-S. Lee, Dynamics of the Bloch point in an asymmetric permalloy disk, Nat. Commun. **10**, 593 (2019).
[17] F. Tejo, J. A. F. Fernandez-Roldan, K. Guslienko, R. M. Otxoa, and O. Chubykalo-Fesenko, Giant supermagnonic Bloch point velocities in cylindrical ferromagnetic nanowires, Nanoscale **16**, 10737 (2024).

[18] C. Sánchez, D. Caso, and F. G. Aliev, Artificial neuron based on the Bloch-point domain wall in ferromagnetic nanowires, Materials **17**, 2425 (2024).

[19] S. K. Kim and O. Tchernyshyov, Pinning of a Bloch point by an atomic lattice, Phys. Rev. B **88**, 174402 (2013).

[20] Z. Gong, J. Tang, S. S. Pershoguba, Z. Xie, R. Sun, Y. Li, X. Yang, J. Liu, W. Zhang, X. Zhang, W. He, H. Du, J. Zang, and Z.-H. Cheng, Current-induced dynamics and tunable spectra of a magnetic chiral bobber, Phys. Rev. B **104**, L100412 (2021).

[21] C. Andreas, A. Kákay, and R. Hertel, Multiscale and multimodel simulation of Bloch-point dynamics, Phys. Rev. B **89**, 134403 (2014).

[22] A. Tapia, C. Saji, A. Roldán-Molina, and A. S. Nunez, Stability enhancement by zero-point spin fluctuations: A quantum perspective on Bloch point topological singularities, Adv. Funct. Mater. **23**, 12721 (2024).

[23] R. G. Elías and A. Verga, Magnetization structure of a Bloch point singularity, Eur. Phys. J. B **82**, 159 (2011).

[24] K. M. Lebecki, D. Hinzke, U. Nowak, and O. Chubykalo-Fesenko, Key role of temperature in ferromagnetic Bloch point simulations, Phys. Rev. B **86**, 094409 (2012).

[25] L. D. Landau and E. M. Lifshitz, On the theory of the dispersion of magnetic permeability in ferromagnetic bodies, Physik. Zeits. Sowjetunion **8**, 153 (1935).

[26] A. Hubert and R. Schäfer, *Magnetic Domains* (Springer, Berlin, 1998).

[27] N. S. Kiselev, Magnoom software (2016), https://github.com/n-s-kiselev/magnoom.

[28] A. S. Savchenko, V. M. Kuchkin, F. N. Rybakov, S. Blugel, and N. S. Kiselev, Chiral standing spin waves in skyrmion lattice, APL Mater. **10**, 071111 (2022).

[29] See Supplemental Material at http://link.aps.org/supplemental/10.1103/PhysRevResearch.7.013195 for the weak-coupling limit in the case $N = 4$; the wave function ansatz for the ground state in the case $N = 4$; the derivation of the intershell interaction Hamiltonian; the asymptotic behavior of the quantum BP profile, its ansatz, and details of the numerical simulations in the $\mathbb{S}_3$-micromagnetic model; the derivation of the SANS cross section for the classical and quantum BPs, which also contains Refs. [39–44].

[30] S. R. White, Density matrix formulation for quantum renormalization groups, Phys. Rev. Lett. **69**, 2863 (1992).

[31] A. Haller, S. Groenendijk, A. Habibi, A. Michels, and T. L. Schmidt, Quantum skyrmion lattices in Heisenberg ferromagnets, Phys. Rev. Res. **4**, 043113 (2022).

[32] I. Dzyaloshinsky, A thermodynamic theory of "weak" ferromagnetism of antiferromagnetics, J. Phys. Chem. Solids **4**, 241 (1958).

[33] T. Moriya, Anisotropic superexchange interaction and weak ferromagnetism, Phys. Rev. **120**, 91 (1960).

[34] E. G. Galkina, B. A. Ivanov, and V. A. Stephanovich, Phenomenological theory of Bloch point relaxation, J. Magn. Magn. Mater. **118**, 373 (1993).

[35] A. S. Savchenko, V. M. Kuchkin, F. N. Rybakov, and N. S. Kiselev, Magnetic bubbles with alternating chirality in domain walls, Front. Phys. **11**, 1223609 (2023).

[36] F. N. Rybakov, N. S. Kiselev, A. B. Borisov, L. Düring, C. Melcher, and S. Blügel, Magnetic hopfions in solids, APL Mater. **10**, 111113 (2022).

[37] T. H. R. Skyrme, A non-linear field theory, Proc. R. Soc. London A **260**, 127 (1961).

[38] V. M. Kuchkin, A. Haller, Š. Liščák, A. Michels, T. L. Schmidt, Manuscript in preparation.

[39] O. M. Sotnikov, E. A. Stepanov, M. I. Katsnelson, F. Mila, and V. V. Mazurenko, Emergence of classical magnetic order from anderson towers: Quantum Darwinism in action, Phys. Rev. X **13**, 041027 (2023).

[40] K. Hesse, I. H. Sloan, and R. S. Womersley, Numerical integration on the sphere, in *Handbook of Geomathematics*, edited by W. Freeden, M. Nashed, and T. Sonar (Springer, Berlin, 2015).

[41] P. Rybakov, Topological excitations in field theory models of superconductivity and magnetism, Ph.D. thesis, KTH Royal Institute of Technology, Stockholm, 2021.

[42] A. Michels, *Magnetic Small-Angle Neutron Scattering: A Probe for Mesoscale Magnetism Analysis* (Oxford University Press, Oxford, 2021).

[43] D. I. Svergun and M. H. J. Koch, Small-angle scattering studies of biological macromolecules in solution, Rep. Prog. Phys. **66**, 1735 (2003).

[44] M. P. Adams, E. P. Sinaga, H. Kachkachi, and A. Michels, Signature of surface anisotropy in the spin-flip neutron scattering cross section of spherical nanoparticles: Atomistic simulations and analytical theory, Phys. Rev. B **109**, 024429 (2024).